Automatic Defect Detection in Leather

João Soares[1], Luís Magalhães[1], Rafaela Pinho[2], Mehrab Allahdad[2] and Manuel Ferreira[2]
[1]*ALGORITMI Research Centre / LASI, University of Minho, Portugal*
[2]*Neadvance, Braga, Portugal*

Keywords: Machine Learning, Leather, Defects Detection, Novelty Detection.

Abstract: Traditionally, leather defect detection is manually solved using specialized workers in the leather inspection process. However, this task is slow and prone to error. So, in the last two decades, distinct researchers proposed new solutions to automatize this procedure. At this moment, there are already efficient solutions in the literature review. However, these solutions are based on supervised machine learning techniques that require a high-dimension dataset. As the leather annotation process is time-consuming, it is necessary to find a solution to overcome this challenge. So, this research explores novelty detection techniques. Moreover, this work evaluates SSIM Autoencoder, CFLOW, STFPM, RDOCE, and DRAEM performances on leather defects detection problem. These techniques are trained and tested in two distinct datasets: MVTEC and Neadvance. These techniques present a good performance on MVTEC defects detection. However, they have difficulties with the Neadvance dataset. This research presents the best methodology to use for two distinct scenarios. When the real-world samples have only one color, DRAEM should be used. When the real-world samples have more than one color, the STFPM should be applied.

1 INTRODUCTION

Leather is a natural material derived from cattle hides through a set of physical and chemical processes. It has been used for a very long time to shield people from the weather, keeping their bodies dry and their temperatures steady. It is still used to create high-quality products like clothing, shoes, purses, and furniture. Because leather is a soft, flexible, and durable material,

In many developing countries, cattle raising plays a critical role in their economic system, being the meat industry the principal economic financial return. However, the value of the cattle hides can represent 3% to 10% of the animal's market value (ALLPI, 2016). So it is important to maximize the leather selling price. At this moment, the following question emerged "What defines the leather selling price?". The main factor is the percentage of defective areas present in a leather piece. The presence of wrinkles, cuts, tick bites, stains, and hot iron marks can reduce the leather piece's selling price. A leather sample with a reduced defective area is beneficial for cattle producers because they sell the leather at a higher price and it is also beneficial for leather goods producers. Because, leather goods produced using non-defective leather reduce the number of defective products, increasing the profit.

Traditionally, the leather inspection process is manual, the workers manipulate the leather samples from distinct points of view to detect defects. Even using specialized workers for this task, the performance of the manual task is low. The defects are very difficult to detect and after some hours of work, the human vision is tired, reducing the defect detection performance. Beyond that, this process is very slow. So, in the last two decades, distinct researchers started to look for automated solutions for these tasks. Using an automated solution, they pretend to increase the number of defects detected and reduce the inspection time.

The related work splits into two: solutions based on Machine Learning (ML) and Deep Learning (DL). The ML solutions extract features using Computer Vision (CV) techniques, like edge detectors and statistical features, to learn to detect defects using supervised ML algorithms. One of the first works applies X^2 criteria to compute the difference between the grey-level histogram of a standard image and an inspected image (Georgieva et al., 2003). This criterion worked because, defective samples generate distinct histograms from the standard histogram, allowing defects detection. Recent research proposes to detect tick bite defects on calf leather (Liong et al., 2019). The authors use hand-crafted feature descriptors to extract local information on leather patches. The hand-crafted fea-

Soares, J., Magalhães, L., Pinho, R., Allahdad, M. and Ferreira, M.
Automatic Defect Detection in Leather.
DOI: 10.5220/0011707000003417
In *Proceedings of the 18th International Joint Conference on Computer Vision, Imaging and Computer Graphics Theory and Applications (VISIGRAPP 2023) - Volume 5: VISAPP*, pages 196-204
ISBN: 978-989-758-634-7; ISSN: 2184-4321
Copyright © 2023 by SCITEPRESS – Science and Technology Publications, Lda. Under CC license (CC BY-NC-ND 4.0)

tures were obtained from statistical approaches like the histogram of pixel intensity values, histogram of oriented gradient, and local binary pattern from edge detector results. The extracted features were combined to detect tick bites using supervised techniques such as decision tree, discriminant analysis, Support Vector Machine (SVM), K-Nearest Neighbor (KNN), and some ensemble classifiers. For the statistical approach, the histogram of pixel intensity values combined with SVM obtains the best result with 80% accuracy. In this research, the authors also experiment with an ANN using ApproxCanny as the preprocessing, obtaining 82.49% classification accuracy. In 2020, statistical techniques are also used to extract local features from image patches (Gan et al., 2020). They obtain the statistical features from the histogram of pixel intensity: median, variance, skewness, kurtosis, lower quartile value, and upper quartile value. After that, the K-S test selects the three representative statistical features from image patches to train a KNN. As a result, the proposed solution obtains an accuracy of 97% in one of the datasets. In another research, the authors present an automated system for detecting and classifying defects (scars, scratches, and pinholes) on the leather surface (Bong et al., 2019). The authors use morphological operations in a pre-processing step to highlight defective regions. Thereafter, the Laplacian operator was applied to threshold the defect boundary. Before the classification task, it was necessary to collect features from the leather images. In that paper, the author extracts features like color moments, color correlograms, and Zernike moments. With these features, it was possible to train a SVM model with a Radial basis kernel to classify defects on the leather surface. This approach obtained a good performance with more than 98% of accuracy. Other solutions emerged in the last years based on DL. In 2020, an experiment ensembled models to automatize the leather inspection (Aslam et al., 2020). Firstly, EfficientNet-B3 and DenseNet-201 were trained from scratch using the skin, concrete, and ImageNet datasets, combining knowledge from distinct domains. After that, the models fine-tune with leather image data. They verified that using transfer learning with the ImageNet dataset had better results than using the skin and concrete dataset. Thus, different models trained by transfer-learning with ImageNet and fine-tuned by leather image data were ensemble because ensemble models obtain a higher accuracy than a single classifier. In the end, they conclude that EfficientNet-B3+ResNext-101 are the best models to ensemble for this problem. Also in 2020, a research suggests a leather defect classification and segmentation system following five steps (Liong et al., 2020). The first is image elicitation where images are captured by a 6-DOF robot arm. In step two, images are selected to remove ambiguity, and in step three images are pre-processed. After that, in step four, the images are annotated to obtain the ground truth labeling to be able to train supervised models. In the end, defect classification and segmentation models are trained and tested. In the classification task, they propose to use a pre-trained network to classify defects in three classes (no defect, black line, and wrinkle). The architecture chosen was AlexNet trained in the ImageNet dataset. The highest three-category classification performance obtained using the proposed method is 95% accuracy. For the segmentation task, convolutional and deconvolutional neural networks were used and the chosen architecture is U-Net. The mean IoU and the mean pixel accuracy achieve are 99% and 99% respectively.

The previously mentioned solutions require a supervised dataset. As dataset acquisition is a time-consuming process and requires specialized workers to annotate the leather samples, supervised techniques are not an option to solve this problem. Beyond that, the leather samples available are unbalanced, and most of the samples are non-defective. So, this work explores an unsupervised approach, known as novelty detection, capable of discriminating anomalous pixels, and learning the non-defective pattern. This work experiments five novelty detection techniques, a reconstruction based technique (Bergmann et al., 2019b), and three Embedding Similarity based techniques: CFLOW (Gudovskiy et al., 2022), Student-Teacher Feature Pyramid Matching (STFPM) (Wang et al., 2021) and Reverse Distillation from One-Class Embedding (RDOCE) (Deng and Li, 2022). Beyond these methodologies, Discriminatively Trained Reconstruction Anomaly Embedding Model (DRAEM) (Zavrtanik et al., 2021) is used to convert the unsupervised problem into a supervised problem to detect defects using supervised architectures. In table 1, there are presented the AUROC results of the mentioned Novelty Detection techniques on Leather MVTEC dataset (Bergmann et al., 2019a).

Table 1: Novelty Detection techniques AUROC results on Leather MVTEC dataset.

Model	Detection	Localization
SSIM AE	-	78.00%
CFLOW	98.26%	98.62%
STFPM	95.50%	97.00%
RDOCE	100%	99.10%
DRAEM	98.0%	97.30%

In summary, the contributions of this research work are listed as follows:

1. A presentation of the disadvantages of the leather detection state-of-art solutions;
2. A presentation of a novelty detection approach and experiments with five novelty detection-based methodologies;
3. A report on the experiments results and present the best methodology for distinct real-world scenarios.

The rest of the paper is structured as follows. Section 2 presents the novelty detection approach in detail. The experiment configuration, such as the two databases used and evaluation metrics, are presented in Section 3. The results are discussed in Section 4 and finally, the conclusions are presented in Section 5, suggesting the methodologies that should be used in distinct scenarios.

2 METHODOLOGY

The novelty detection approach was developed to solve problems like this, where the presence of anomalous samples (outliers) are rare. The novelty detection techniques learn the pattern from the unsupervised dataset samples. As most of the data elements from the real-world scenario are non-defective (inliers), the novelty detection technique learns the inlier's sample pattern (Bergmann et al., 2019a). This approach can also be used to detect defects in images. In this case, the novelty techniques learn to produce anomaly score maps using non-defective images. In the inference phase, when the technique is presented with defective images, the anomaly score maps produced should attribute high scores to the unknown patterns, in other words, to the defective regions. The novelty detection techniques have two main categories: Reconstruction-based and Embedding Similarity based. Reconstruction-based techniques learn to encode and reconstruct inlier samples and should fail on outliers sample reconstruction. In this approach, architectures like Autoencoders (AE), Variational AE, and Generative Adversarial Networks can be used to reconstruct the image samples. The reconstruction methods can localize the anomalies using pixel error or a structural similarity function. On other hand, the Embedding Similarity-based techniques use pre-trained DL networks to extract image features. After that, the extracted features are combined to create an anomaly score map. One advantage of the embedding methods is the different layers of vector extraction. In this way, if the output extracted is from the first layers, the features obtained will represent small defects. If the extracted output is from the last layers, the obtained features will represent large defects.

3 EXPERIMENTS

In this research, to evaluate the novelty detection techniques, there are proposed three distinct experiments using the Novelty Detection techniques:

- **Experiment 1** - Train and evaluate the techniques with MVTEC dataset and with Neadvance dataset;
- **Experiment 2** - Train with MVTEC dataset and evaluate with Neadvance dataset, and vice versa;
- **Experiment 3** - Train the techniques with both datasets and evaluate for MVTEC and Neadvance datasets;

The first experiment is a baseline experiment to evaluate the ability of the Novelty Detection techniques detects defects with the same leather pattern as used during the training. The second experiment is performed to evaluate the generalization ability of these techniques. Check if the techniques can detect defects from samples with different patterns than the used during the training. The third experiment was performed to verify if a larger dataset, combining the color patterns from both datasets can obtain better results than Experiment 1.

3.1 Datasets

In this research, two different datasets were used to apply novelty detection techniques. One is made up of the leather samples from MVTec AD dataset, while the other is a dataset created using images captured by Neadvance. MVTec AD is a dataset for anomaly detection. It has been used as a benchmark image dataset in the most current researches. It includes leather samples and has 5000 images distributed over fifteen different categories. There are 123 images for testing and 235 images for training in the MVTec leather dataset. There are 42 normal images in the test dataset, 19 with color defects, 19 with cut defects, 17 with fold defects, 19 with glue defects, and 17 with poke defects. There is a ground truth mask for each test image. The test dataset of this dataset only contains 2.7 percent anomalous pixels. There is an image of each MVTEC defect type in Figure 1

Using the Neadvance defective images and the corresponding annotations, the second dataset was created. It has 211 defective images, 40 with cut defects, 47 with hole defects, 52 with line defects, and 82 with wrinkle defects. Non-defective samples

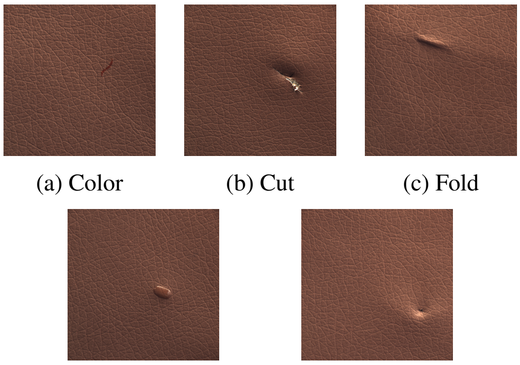

(a) Color (b) Cut (c) Fold

(d) Glue (e) Poke

Figure 1: MVTEC leather defect samples.

are not present in the initial dataset. In order to create non-defective samples, the non-defective regions from the defective samples were cropped. 42 and 260 non-defective areas, respectively, were cropped for testing and training. The 211 defective samples and 42 non-defective regions compose the testing dataset. The defects shown in this dataset are harder to find than MVTEC. There is an illustration of each Neadvance defect type in the Figure 2.

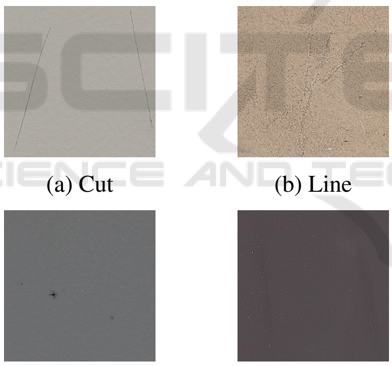

(a) Cut (b) Line

(c) Hole (d) Wrinkle

Figure 2: Neadvance leather defect samples.

3.2 Metrics

In this study, selecting the appropriate evaluation metrics is critical for evaluating the presented approaches. For this problem, it is important to evaluate two tasks, defects localization (segmentation) and detection (binary classification). One of the metrics employed for the localization task is Intersection Over Union (IOU), a popular metric for segmentation problems. Per-region Overlap (PRO) is also used, it is popular in others anomaly detection researches, such as (Defard et al., 2021). PRO instead of treating every pixel as independent, averages the performance over each connected component of the ground truth (Bergmann et al., 2021). IoU and PRO are threshold dependent, in other words, require a threshold to binarize the anomaly score maps to obtain the predicted mask. To evaluate the techniques independently of the estimated threshold, it is used the Area Under Receiver Operating Characteristic Curve (AUROC). Additionally, the AUROC is utilized to evaluate the defects detection task, comparing the maximum value of the anomaly scores map with the ground truth label (defective or not). Furthermore, because the measure was threshold dependent, F1-Score was selected, which considered as defective every predicted mask with at least one defective pixel.

3.3 Thresholds

For these experiments, three distinct thresholds are used. Using a small sample of training images, the p-Quantile was used to estimate the first threshold (T1). The p-Quantile chooses a threshold such that a percentage p of the threshold distribution pixels are classified as being free of anomalies (outlier). The p-value for this method was set at 99, which is the state of the art for outlier detection. The second and third thresholds (T2 and T3) use the small set of the testing dataset to estimate a threshold that optimizes the F1-Score for localization and defects detection, respectively. Using the source code from the Gudovskiy repository [1], T2 and T3 are estimated.

SCITEPRESS SCIENCE AND TECHNOLOGY PUBLICATIONS

3.4 Training and Evaluation Setup

In this experiment, the techniques are trained using 70% of the training dataset. The techniques train utilizing reshaped 256*256 pixel images over 300 iterations at a learning rate of 0.01. The remaining 30% of non-defective images are divided in half, and 15% are used for model validation to save checkpoints and verify early stopping. The remaining 15% is needed to calculate T1. 15% of the testing dataset is used to estimate T2 and T3. ResNet18 was selected to work as a feature extractor because CFLOW, STFPM, and RDOCE require for a pre-trained backbone. Each of the methodologies presented has unique memory needs because each has a different architecture. Consequently, each will have a unique batch size. The hardware set up of the machine will be used to perform this experiment is Intel(R) Xeon(R) CPU E5-2680 V4@2.4GHZ and NVIDIA GeForce GTX 1080Ti 11 GB.

[1] https://github.com/gudovskiy/cflow-ad

4 RESULTS

In this section, the results of three experiments are presented. Only for the Experiment 1 are presented the quantitative, qualitative and complexity results. For Experiment 2 and Experiment 3 the quantitative results are presented.

4.1 Experiment 1 - Quantitative Results

The localization and detection results of all techniques' are compared in Table 2 using the MVTEC dataset. CFLOW has the greatest AUROC of any of the localization results, at 99.57%, followed by RDOCE and STFPM, at 99.31% and 98.91%, respectively. It is evident from the IoU results analysis that segmentation T2's optimized threshold yields superior outcomes to T1's. Almost all techniques have higher IoU using T2 than T1. T1 outperforms T2 in PRO columns results, with the exception of DRAEM. These results demonstrated how important the threshold estimation process is. The DRAEM AUROC is 4% less than the CFLOW. However, DRAEM uses T2 to show the best IoU result.

Looking for the MVTEC detection columns, CFLOW outperforms all the other techniques with 100% AUROC and 95.36% F1-Score using T3. The SSIM approach yields the lowest results, however the MVTEC outcomes for both tasks appear to be similar. It performs better in this experiment than the early studies. SSIM AE had 94.18% AUROC in this experiment, compared to 78% AUROC in the original article. This happens because the used architecture segment borders as defective. Therefore, a clean border method was used, which raised AUROC.

The quantitative results utilizing the Neadvance dataset are shown in Table 3. It may be confirmed that the AUROC results are inferior to the MVTEC results by analyzing the segmentation metrics. With 72.52%, 71.40%, and 74.17% of AUROC, respectively, CFLOW, STFPM, and Reverse continue to perform better than the other approaches, just as with MVTEC. In contrast to MVTEC, DRAEM achieves an extremely low AUROC of 46.77%. The IoU values are quite poor, which indicates that the expected and ground truth masks are very unlike.

STFPM, RDOCE, and DRAEM perform better than the other approaches in the Neadvance detection results columns with 77.41%, 77.05%, and 77.74% AUROC, respectively. On F1-Score, DRAEM does not consistently achieve good results. DRAEM has an F1-Score of 1.08% using T1 and 4.39% using T2. F1-Score does not show any appreciable differences between thresholds for detection.

4.2 Experiment 1 - Qualitative Results

Performance of the novelty detection techniques are measured using evaluation metrics. Beyond that, it is a good habit to use visual examples to confirm the effectiveness of the strategies. Figure 3 and Figure 4 present one anomaly score map and mask (denoted with a red line) by each technique using an MVTEC and Neadvance sample. The predicted mask is obtained using the segmentation optimized T2.

It may be confirmed through analysis of the MVTEC sample results that all techniques detect and locate the defective region. The best masks are produced by DRAEM because the anomaly scores map clearly defines the defective boundaries. It assigns a high score to the defective area and a low score to the normal area. CFLOW anomaly map gives high scores to non-anomalous regions. However, they are not thresholded as anomalous. The Neadvance sample results only detect the defective region using SSIM AE, STFPM, and RDOCE. DRAEM provides an excellent anomaly scores map using the MVTEC sample. However, with the Neadvance sample, DRAEM attributes high scores to every pixel, impeding the defect threshold. The SSIM AE anomaly scores map shows other locations with high scores, and it also classifies non-defective regions as defective.

4.3 Experiment 1 - Complexity Results

In real-time solutions, the complexity of each technique is crucial. To work in real-time, the number of predicted frames per second (FPS) has to be high as possible. It appears from an analysis of the table 4 that MVTEC takes longer to make inferences than the Neadvance dataset. This fact is caused by the MVTEC batch loading time. As the MVTEC images have 1024*1024 resolution and the Neadvance images have 256*256 resolution, the batch loading spends more time because it has to resize the MVTEC images to the 256*256 resolution. The DRAEM approach was the fastest in this experiment, achieving 56.10 FPS when using the Neadvance dataset and 34.69 FPS while using the MVTEC. Because DRAEM does not extract features to create the anomalous score map. And these operations increase the inference time, reducing the number of FPS. The smaller number of FPS from the RDOCE technique, when compared with STFPM, can be caused by the increased complexity of using OCBE architecture.

Table 2: MVTEC dataset results.

	Localization Metrics (%)					Detection Metrics (%)		
Model	IoU T1	IoU T2	PRO T1	PRO T2	AUROC	F1-Score T1	F1-Score T3	AUROC
SSIM AE	31.33	29.41	47.24	42.01	94.18	92.13	90.57	91.38
CFLOW	7.28	22.54	99.98	95.65	99.57	82.02	95.36	100
STFPM	4.39	22.32	99.42	43.16	98.91	46.60	86.76	97.08
RDOCE	1.23	21.49	99.99	79.81	99.31	68.92	91.67	99.91
DRAEM	1.49	38.97	2.34	75.49	94.8	63.06	88.76	99.23

Table 3: Neadvance dataset results.

	Localization Metrics (%)					Detection Metrics (%)		
Model	IoU T1	IoU T2	PRO T1	PRO T2	AUROC	F1-Score T1	F1-Score T3	AUROC
SSIM AE	6.24	0.65	12.04	32.63	68.07	53.13	55.51	62.95
CFLOW	1.92	0.01	14.27	17.11	72.52	70.51	70.53	70.79
STFPM	2.18	7.61	8.03	48.26	71.40	21.78	33.03	77.41
RDOCE	4.78	9.89	51.71	28.03	74.17	70.75	70.75	77.05
DRAEM	0.01	0.01	72.37	82.43	46.77	1.08	4.39	77.74

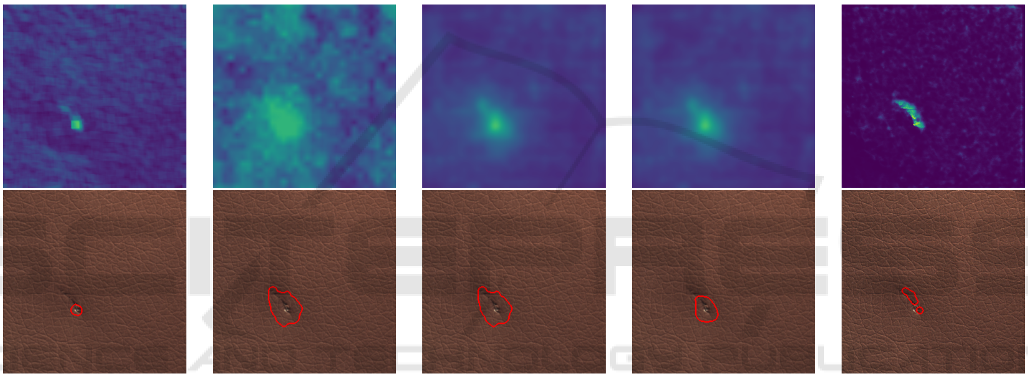

(a) SSIM AE (b) CFLOW (c) STFPM (d) RDOCE (e) DRAEM

Figure 3: MVTEC leather maps and masks.

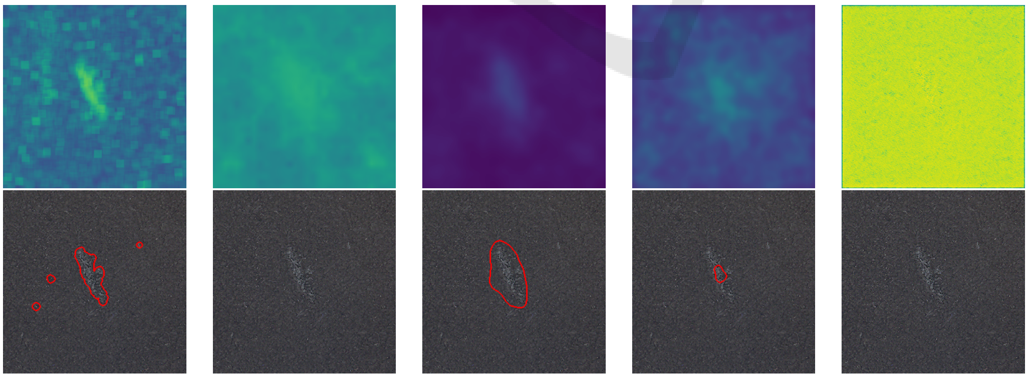

(a) SSIM AE (b) CFLOW (c) STFPM (d) RDOCE (e) DRAEM

Figure 4: Neadvance leather maps and masks.

4.4 Experiment 2 - Quantitative Results

Table 5 shows the results of the MVTEC dataset using models trained on the Neadvance dataset. The AUROC results for SSIM AE, CFLOW, STFPM, and Reverse (95.06%, 97.89%, 91.93%, and 94.27%) appear to be good and are equivalent to those from table 2. DRAEM experienced the biggest drop in AUROC,

Table 4: Complexity results (MVTEC/Neadvance).

Model	Inference time	FPS
SSIM AE	4.24 / 5.84	29.28 / 43.31
CFLOW	10.29 / 12.63	12.04 / 20.02
STFPM	5.63 / 6.17	21.99 / 40.96
RDOCE	10.62 / 16.9	11.66 / 14.89
DRAEM	3.57 / 4.50	34.69 / 56.10

from 94.80% to 38.79%. The inability of DRAEM to learn the Neadvance features can be used to explain this decline. For the majority of the techniques, the outcomes are incredibly poor when compared to the threshold-dependent metrics. According to the information in this table, SSIM AE achieves 15.02% IoU using T1, 33.27% IoU using T2, 19.45% PRO using T1, and 46.02% using T2. Based on this table, certain models can generalize if they only identify the best thresholds for the testing dataset.

Table 5 shows the results for the defects detection task on the MVTEC dataset using Neadvance as the training dataset, which are now prepared for analysis. Unexpectedly, with 95.82% AUROC, SSIM AE beats all other techniques. DRAEM also claims attenction because, it achieves the worst AUROC of all techniques. With T3, the SSIM produces the best results for the F1-Score.

The Neadvance results using MVTEC as the training dataset are shown in table 6. The results shown in this table for the localization metrics are poor, mirroring those from table 3. The AUROC results have once more shown a slight decrease in the majority of the models (from 68.07%, 72.52%, 71.40%, 74.17%, and 46.77%).

Even though they weren't trained on the Neadvance dataset, the detection metrics SSIM AE and DRAEM in this table match to the AUROC results of table 3. This table shows the respective AUROC for SSIM AE and DRAEM at 62.14% and 77.74%. It is crucial to call attention to the SSIM AE results for F1-Score in this table, which are 51.16% for T1 and 62.28% for T3. The Neadvance dataset produced better results than the table 3, with 53.13% for T1 and 55.51% for T3.

4.5 Experiment 3 - Quantitative Results

In order to analyze the MVTEC results utilizing models trained using MVTEC and Neadvance, let's first look at the results of table 7. The majority of the techniques produce excellent AUROC values for localization metrics, following the AUROC results of table 2. The DRAEM AUROC performance in this table is unsatisfactory. DRAEM AUROC decreases by about 40% when compared to table 2. The inability of DRAEM to learn the Neadvance samples, as displayed in table 3, can be used to explain this decline. The outcomes of the threshold-dependent metrics can now be examined. With a 35.44% IoU, SSIM AE uses T2 to produce the best result for the IoU metric. Additionally, utilizing T2, SSIM AE was the method that produced the best results for the PRO metric, with a result of 57.13%.

The results of this table do not match the MVTEC detection results from table 2 in terms of MVTEC detection results. SSIM AE and CFLOW nonetheless achieve good AUROC values of 92.30% and 99.73%, respectively, despite the AUROC results not being as high as previously. The F1-Score results utilizing T3 on the other hand, produce good results that are comparable to those shown in table 2. The F1-Score results utilizing T3 outperform the prior results for SSIM AE and CFLOW, increasing the SSIM AE F1-Score value from 90.57 to 93.59 and the F1-Score from 95.36 to 95.95%.

The results of Neadvance localization utilizing methods developed with MVTEC and Neadvance are shown in table 8. This table appears to match the AUROC results from table 3 in terms of localization metrics. For SSIM AE, the AUROC rises from 68.07% to 71.26 %. Additionally, it rises from 72.52% to 74.35% in the case of CFLOW. The STFPM and Reverse AUROC values, however, decline. The STFPM AUROC decreased from 71.40% to 66.69% then Reverse from 74.17% to 73.25%. It appears that using this technique on both datasets did not enhance the localization results. This can be explained by how challenging it is to detect Neadvanced defects.

Relatively to the Neadvance detection using techniques trained with MVTEC and Neadvance, it presents satisfactory AUROC results, achieving the maximum with DRAEM, 78.69%. These results outperform the AUROC results when compared to those shown in table 3. T3 values from SSIM AE, CFLOW, STFPM, and Reverse are superior to those from the F1-Score. Additionally, the T1 now has SSIM AE, STFPM, and DRAEM enhancements.

5 CONCLUSIONS

Relatively to the Experiment 1, the ideas that arise from the previous analyzes are that SSIM AE presents the worst quantitative results. Compared with the other techniques, SSIM AE only has a good inference time. Even though, DRAEM outperforms SSIM AE complexity results. As seen in the quantitative and qualitative results, DRAEM performs very well in the MVTEC dataset. However, it has a horrible

Table 5: MVTEC dataset results using models trained with Neadvance.

	Localization Metrics (%)					Detection Metrics (%)		
Model	IoU T1	IoU T2	PRO T1	PRO T2	AUROC	F1-Score T1	F1-Score T3	AUROC
SSIM AE	15.02	33.27	19.45	46.09	95.06	71.33	83.02	95.82
CFLOW	0.01	1.73	0	0	97.89	0	0	89.37
STFPM	4.26	3.54	6.43	4.23	91.93	57.75	0	63.32
RDOCE	0.01	1.30	5.89	9.23	94.27	0	0	68.61
DRAEM	0.02	0.42	7.14	9.05	38.79	4.25	0	41.00

Table 6: Neadvance dataset results using models trained with MVTEC.

	Localization Metrics (%)					Detection Metrics (%)		
Model	IoU T1	IoU T2	PRO T1	PRO T2	AUROC	F1-Score T1	F1-Score T3	AUROC
SSIM AE	1.07	3.68	9.80	7.19	61.07	51.16	62.28	62.14
CFLOW	0.07	0.02	0	0	50.77	0	0	46.66
STFPM	0.04	4.89	3.11	4.51	57.06	0	0	69.41
RDOCE	0.04	0.02	8.82	6.37	69.05	0	0	58.36
DRAEM	0.05	0.02	5.42	7.62	47.90	2.80	0	77.74

Table 7: MVTEC dataset results using models trained with MVTEC and Neadvance.

	Localization Metrics (%)					Detection Metrics (%)		
Model	IoU T1	IoU T2	PRO T1	PRO T2	AUROC	F1-Score T1	F1-Score T3	AUROC
SSIM AE	23.14	35.44	31.74	57.13	91.02	77.78	93.59	92.30
CFLOW	1.34	23.08	0	9.62	99.52	77.78	93.59	92.30
STFPM	14.19	21.47	59.80	23.70	96.46	79.17	77.61	81.17
RDOCE	9.06	22.70	41.76	49.28	99.93	83.62	80.00	77.85
DRAEM	0.14	1.43	0.12	2.81	55.09	22.99	0	55.80

Table 8: Neadvance dataset results using models trained with MVTEC and Neadvance.

	Localization Metrics (%)					Detection Metrics (%)		
Model	IoU T1	IoU T2	PRO T1	PRO T2	AUROC	F1-Score T1	F1-Score T3	AUROC
SSIM AE	5.57	6.77	26.9	14.83	71.26	66.90	60.15	68.65
CFLOW	0.01	3.03	0	32.87	74.35	0	80.69	73.30
STFPM	4.24	6.51	9.03	15.96	66.69	38.63	35.40	67.42
RDOCE	3.01	7.71	21.93	32.12	73.25	70.13	85.39	66.30
DRAEM	0.01	0.01	0.01	9.68	54.01	36.30	0	78.69

performance with the Neadvance dataset. The bad results could be justified by the inability of the DRAEM to learn to segment the samples from distinct colors. So, DRAEM should be an option when the real-world scenario samples have only one color. The three feature-extraction-based methodologies achieve great results. The CFLOW is the technique in the state-of-the-art with the highest segmentation AUROC for the MVTEC dataset and this experiment confirms that. In this experience, the CFLOW has 100% of detection AUROC with the MVTEC samples. However, CFLOW does not produce the best anomaly score maps, difficulting the scores maps threshold. The STFPM and RDOCE are two teacher-student architectures. As RDOCE uses an OCBE, the time complexity increases relatively to STFPM. These two techniques have similar quantitative results for both datasets. Analyzing the previous arguments, the STFPM is the best option of these three techniques. It has a higher number of predicted FPS and achieves similar results, outperforming the previous techniques as analyzed in the qualitative results. So, in cases such as the Neadvance where DRAEM is not an option, STFPM should be used.

Relatively to the Experiment 2, it seems that there is generalization ability in the novelty detection techniques. In this way it is possible to use a novelty technique to detect defects different from the used during the training. However, the results are better when the the techniques are trained with samples that follow the real world scenario pattern.

Relatively to the Experiment 3, the increasing of training complexity caused by the increasing number of training samples did improve the evaluation metrics results. So, it is recommended to train a novelty detection technique for each real world scenario. In this way, the technique can be optimized for samples with the same features as the training samples.

The work presented in this paper solves the leather detection problem. However, every day, new researches present novelty detection methodologies that overcome the previous state-of-the-art techniques. So, for future work, the continuous upgrading of leather detection solutions using recent novelty detection methodologies is mandatory. New ways to estimate the binary threshold, to convert the anomaly score maps into a binary mask, should also be explored. Also, it is crucial to continue looking for solutions with low computation requirements. Most of the time, these solutions are applied in small computers that do not have the required hardware to implement the methodologies. On other hand, the presented solutions can perform better if the training dataset was bigger. In this way, it is necessary to invest in leather image capture.

ACKNOWLEDGEMENT

This work is supported by: European Structural and Investment Funds in the FEDER component, through the Operational Competitiveness and Internationalization Programme (COMPETE 2020) [Project nº 42778; Funding Reference: POCI-01-0247-FEDER-042778].

REFERENCES

ALLPI (2016). Africa leather and leather products institute - hides and skins improvement handbook: Trainer's manual - hides and skins improvement handbook: Trainer's manual.

Aslam, M., Khan, T. M., Naqvi, S. S., Holmes, G., and Naffa, R. (2020). Ensemble convolutional neural networks with knowledge transfer for leather defect classification in industrial settings. *IEEE Access*, 8:198600–198614.

Bergmann, P., Batzner, K., Fauser, M., Sattlegger, D., and Steger, C. (2021). The mvtec anomaly detection dataset: A comprehensive real-world dataset for unsupervised anomaly detection. *International Journal of Computer Vision*, 129:1038–1059.

Bergmann, P., Fauser, M., Sattlegger, D., and Steger, C. (2019a). Mvtec ad-a comprehensive real-world dataset for unsupervised anomaly detection. *Proceedings of the IEEE Computer Society Conference on Computer Vision and Pattern Recognition*, 2019-June:9584–9592.

Bergmann, P., Löwe, S., Fauser, M., Sattlegger, D., and Steger, C. (2019b). Improving unsupervised defect segmentation by applying structural similarity to autoencoders. In *Proceedings of the 14th International Joint Conference on Computer Vision, Imaging and Computer Graphics Theory and Applications*. SCITEPRESS - Science and Technology Publications.

Bong, H. Q., Truong, Q. B., Nguyen, H. C., and Nguyen, M. T. (2019). Vision-based inspection system for leather surface defect detection and classification. *NICS 2018 - Proceedings of 2018 5th NAFOSTED Conference on Information and Computer Science*, pages 300–304.

Defard, T., Setkov, A., Loesch, A., and Audigier, R. (2021). Padim: a patch distribution modeling framework for anomaly detection and localization. In *International Conference on Pattern Recognition*, pages 475–489. Springer.

Deng, H. and Li, X. (2022). Anomaly detection via reverse distillation from one-class embedding. In *Proceedings of the IEEE/CVF Conference on Computer Vision and Pattern Recognition*, pages 9737–9746.

Gan, Y. S., Chee, S.-S., Huang, Y.-C., Liong, S.-T., and Yau, W.-C. (2020). Automated leather defect inspection using statistical approach on image intensity. *Journal of Ambient Intelligence and Humanized Computing 2020 12:10*, 12:9269–9285.

Georgieva, L., Krastev, K., and Angelov, N. (2003). Identification of surface leather defects. In *CompSysTech*, volume 3, pages 303–307. Citeseer.

Gudovskiy, D., Ishizaka, S., and Kozuka, K. (2022). Cflow-ad: Real-time unsupervised anomaly detection with localization via conditional normalizing flows. In *2022 IEEE/CVF Winter Conference on Applications of Computer Vision (WACV)*, pages 1819–1828.

Liong, S., Zheng, D., Huang, Y.-C., and Gan, Y. (2020). Leather defect classification and segmentation using deep learning architecture. *International Journal of Computer Integrated Manufacturing*, 33:1–13.

Liong, S.-T., Gan, Y. S., Huang, Y.-C., Liu, K.-H., and Yau, W.-C. (2019). Integrated neural network and machine vision approach for leather defect classification. *arXiv preprint arXiv:1905.11731*.

Wang, G., Han, S., Ding, E., and Huang, D. (2021). Student-teacher feature pyramid matching for unsupervised anomaly detection. *arXiv preprint arXiv:2103.04257*.

Zavrtanik, V., Kristan, M., and Skocaj, D. (2021). Draem - a discriminatively trained reconstruction embedding for surface anomaly detection. In *Proceedings of the IEEE/CVF International Conference on Computer Vision (ICCV)*, pages 8330–8339.